# Synthesis and characterization of uniform nanoparticles of $\gamma$-Mo$_2$N for supercapacitors

LI Xue-liang(李学良)[1, 2], XING Yan(邢 妍)[1, 2], WANG Hua(汪 华)[1, 2],
WANG Hua-lin(王华林)[1, 2], WANG Wei-dong(王维东)[1, 2], CHEN Xiang-ying(陈祥迎)[1, 2]

1. School of Chemical Engineering, Hefei University of Technology, Hefei 230009, China;
2. Anhui Key Laboratory of Controllable Chemical Reaction and Material Chemical Engineering,
Hefei University of Technology, Hefei 230009, China

**Abstract:** Uniform nanoparticles of molybdenum nitride were synthesized by temperature-programmed reaction(TPR) using MoO$_3$ and ammonia as reactants. This material was characterized by X-ray diffractometry(XRD), transmission electron microscopy(TEM), scanning electron microcopy(SEM) and cyclic voltammetry(CV). Results show that the material consists of a pure phase of $\gamma$-Mo$_2$N nanoparticles with average diameter of about 16 nm. The material presents a specific capacitance of 172 F/g in 1 mol/L H$_2$SO$_4$ electrolyte at a scan rate of 1 mV/s and the potential window is broadened to 1.1 V (−0.6 to 0.5 V). At the 6 000th cycle, the material remains 94.9% and 94.7% of the initial capacitance in 1 mol/L H$_2$SO$_4$ and KCl solution, respectively. A possible mechanism comprising surface control and diffusion control is proposed to explain the effect of scan rates on specific capacitance.
**Key words:** molybdenum nitride; cyclic voltammetry; specific capacitance; scan rate

## 1 Introduction

Supercapacitors are new charge storage devices with a higher energy density than conventional dielectric capacitors and with a higher power density than batteries. They typically exhibit 20−200 times greater capacitance per unit volume or mass than conventional capacitors[1] and have important application in products as diverse as cardiac pacemakers, cellular phones, electric vehicles and so on[2].

Many kinds of metal compounds, such as metal oxides and metal nitrides, have been used as the supercapacitor electrode materials. Metal oxides include MnO$_2$[3−4], NiO[5], RuO$_2$[6] and so on. The supercapacitors consisting of hydrous ruthenium oxides exhibit very large pseudocapacitance and good reversibility[7−9], but the high cost of ruthenium precursors has limited their commercial attraction. Therefore, considerable efforts have been devoted to the development and characterization of new electrode materials with lower cost and better performance, so

cheap candidates with good capacitive characteristics have attracted much attention. Since pseudocapacitance mainly comes from the reversible redox reactions of the electroactive materials, some nonferrous metal compounds, such as Ni(OH)$_2$[10], Mo$_2$N[11−12], VO$_2$[13], are considered to be promising materials applicable in supercapacitors.

There are a lot of studies on the $\gamma$-Mo$_2$N[14−16] employed as an active catalyst for hydrodenitrogenation and hydrodesulphurization, etc. For example, NAGAI et al[14] and KIM et al[17] made much contribution in this field. However, there are a few reports about $\gamma$-Mo$_2$N applied as charge storage materials. Owing to the high activity and high specific surface area, it is not surprising that the application of molybdenum nitride in supercapacitors material has also been considered. To further demonstrate the effect of the scan rate, LIU et al[18] explored the relationship between specific capacitance and scan rate, however, they did not offer a specific capacitance value of molybdenum nitrides. The highest capacitance of the composite material of molybdenum nitride reported by CHEN et al[12] reached

109.9 F/g. Particle diameter of metal compounds may play an important role in improving the electrochemical characteristics. Super-fine nanoparticles have much larger specific area, so, they can also support higher specific capacitance. To further investigate these factors of electrochemical performance, on the basis of the previous researches, we synthesized super fine particles of $\gamma$-Mo$_2$N by temperature-programmed reaction(TPR) using MoO$_3$ and ammonia as the reactants, and studied electrochemical characteristics in different aqueous electrolytes.

## 2 Experimental

### 2.1 Chemicals

All the analytical reagents were purchased from Shanghai Chemical Reagent Company, China, and used without further purification. The purity of NH$_3$ was 99.99%. Water used in all experiments was doubly distilled. All electrochemical experiments were carried out at room temperature.

### 2.2 Synthesis

1.18 g MoO$_3$ was placed on a porcelain boat in a quartz tube and nitrided by temperature-programmed reaction(TPR) with ammonia gas (NH$_3$) (99.99%) in vacuum system. At the rate of 1 K/min, the temperature raised from room temperature to 973 K , and the system was kept at this temperature for 2 h. Then it was slowly quenched to room temperature naturally and kept for 12 h. The sample was put in the desiccator and kept in reserve for use. The NH$_3$ flow rate was adjusted to yield mass space velocity up to 1.6 mL/s.

### 2.3 X-ray diffraction

X-ray diffraction measurements were made with a Rigaku D/max-rB X-ray diffractometer operating at a scanning speed of 2($^\circ$)/min using Cu K$_\alpha$ radiation ($\lambda$= 0.154 06 nm). The crystallite size, $D_c$, was determined by the Scherrer's equation[19], $D=K\lambda/(B\cdot\cos\theta)$, where $\lambda$ is the corrected wavelength of the X-radiation, $B$ is the full width at half maximum corrected for instrumental broadening, and $\theta$ is the Bragg angle of the diffraction peak.

### 2.4 Morphology investigation

The morphology of material was characterized by Hitachi Model H-800 transmission electron microscope with an accelerating voltage of 200 kV and by (FE-SEM, FEI Sirion200) scanning electron microscope. The sample was crushed using an agate pestle and mortar dispersed in alcohol with an ultrasonic apparatus, placed on a microgrid of silicon, and transferred to the analysis

chamber in SEM equipment.

### 2.5 Electrode preparation and electrochemical characterization

The titanium sheets were previously etched by ultrasonic in 0.1 mol/L HCl solution at room temperature for 20 min to remove oxide layers, and then rinsed with doubly distilled water and dried in a vacuum oven at 373 K for 12 h. The electrode material was a mixture of $\gamma$-Mo$_2$N, acetylene black and polyvinylidene difluoride (PVDF) with a mass ratio of 85:10:5. The solvent was dropped into the above mixture and ground to form the coating slurry. And this slurry was smeared onto the pretreated titanium sheet (40 mm$\times$20 mm) that serviced as current collector, and then the electrode was dried in a vacuum oven at 423 K for 2 h.

Characterization of electrochemical capacitor performance was conducted by means of cyclic voltammetry(CV) and A.C. impedance. The electro-chemical experiments were performed on an electro-chemical analyzer system, CHI660B microcomputer-based electrochemical analyzer. All measurements were carried out in a conventional three-compartment cell. A platinum foil was used as counter electrode. All potentials were referenced to saturation calomel electrode(SCE).

## 3 Results and discussion

### 3.1 XRD characterization

The typical XRD pattern of the molybdenum nitride prepared by temperature-programmed reaction(TPR) is shown in Fig.1. Intensive and broad peaks are observed at $2\theta$=37.38$^\circ$, 43.45$^\circ$, 63.11$^\circ$ and 75.73$^\circ$, which are close to JCPDS standard $\gamma$-Mo$_2$N (No.25−1366). Therefore, the as-prepared material is $\gamma$-Mo$_2$N. This indicates the high purity of the final product with no other phase detected. According to Scherrer's equation, $D=K\lambda/(B\cdot\cos\theta)$, the average diameter of the particles is about 16 nm.



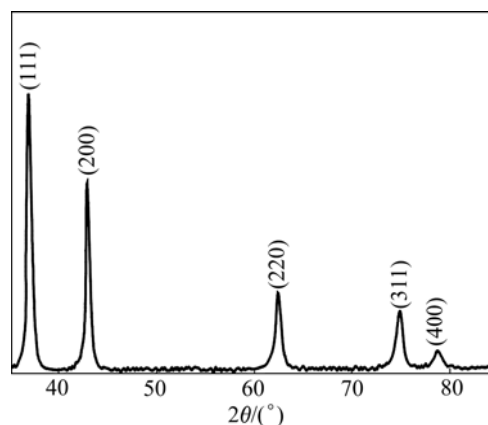**Fig.1** XRD pattern of as-prepared material

## 3.2 Morphology of as-prepared material

A typical TEM image of the as-prepared material is shown in Fig.2. From the image, the particles with a uniform size of about 50 nm are shown. The results are larger than those from XRD using Scherrer's equation for the peaks. The aggregation of particles is observed in some parts of the sample.
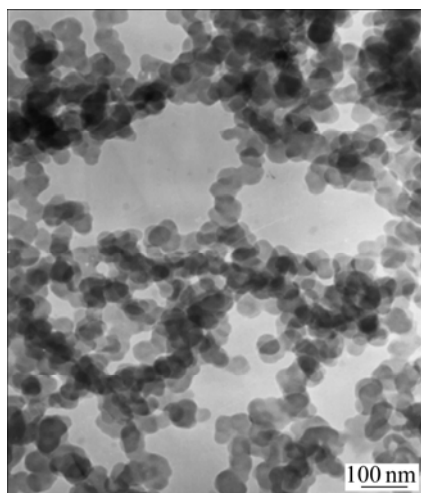


**Fig.2** TEM image of sample

SEM image of the as-prepared material is shown in Fig.3. The aggregation of particles is also observed in some parts of Fig.3, while small particles (calculated 16 nm) are partially agglomerated. Fig.3 shows that the particles have an average diameter of about 50 nm, which is almost in accordance with TEM result. It is obvious that the particles (calculated 50 nm) are larger than the results ($D_c$=16 nm) from the XRD using Scherer's equation for the peaks at $2\theta$=37.10˚ due to the aggregation of primary particles during the synthesis procedure.
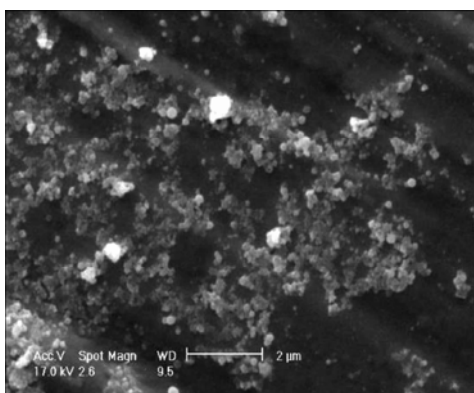


**Fig.3** SEM image of sample

## 3.3 Capacitance performance

### 3.3.1 Typical CV curves

Typical CV curves shown in Fig.4 represent the behavior of $\gamma$-Mo$_2$N in 1 mol/L H$_2$SO$_4$ at different scan rates. The value of specific capacitance is determined by the equation as follows:

$$C=\Delta I/(2\cdot v\cdot m) \tag{1}$$

where $C$ is the specific capacitance; $\Delta I$ is the average current; $v$ is the voltage-sweeping rate; $m$ is the mass of the active material in an electrode. In Fig.4, negative direction stands for oxidation current and positive one stands for reduction current. Ideal CV curves of electrochemical supercapacitor material should be standard rectangular current—potential response curves. The material shows good supercapacitive performance from −0.6 to 0.5 V (vs SCE) and has approximately rectangular current—potential response curves.
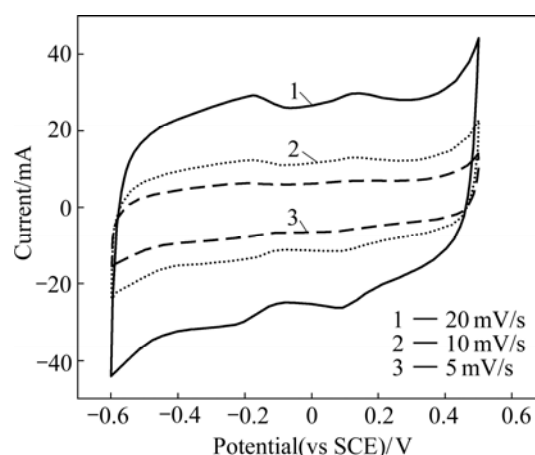


**Fig.4** Typical CV curves of $\gamma$-Mo$_2$N in 1 mol/L H$_2$SO$_4$ at different scan rates

### 3.3.2 Effect of scan rate on specific capacitance

The specific capacitances of $\gamma$-Mo$_2$N were measured in different cases. By changing the scan rate of potential, the effect of scan rate on the specific capacitance in 1 mol/L H$_2$SO$_4$ was studied. Fig.5 presents the values of specific capacitance at different rates, where $C$ is the capacitance and $v$ is the scan rate.

For a mixed process, whether it involves a surface mechanism (d$i$/d$v$=constant=the capacitance) or a diffusion controlled mechanism (d$i$/d$v^{1/2}$=constant), it can be simulated by this equation:

$$C=k_1+ \ k_2/v^{1/2} \tag{2}$$

from which $k_1$ and $k_2$ can be calculated if $C$, when plotted vs $v^{-1/2}$, gives a straight line with slope $k_2$ and intercept $k_1$[18].

LIU et al[18] explored and made much development to the relationship between scan rate and specific capacitance; however, no simple mechanism for the origin of the scan rate dependence of the response currents could be found.

The relationship between scan rate and specific capacitance of the as-prepared material is given in Fig.5.

When the scan rate is less than 5 mV/s, a straight line with slope $k_d$ is obtained; while the rate is more than 10 mV/s, another one with slope $k_e$ is obtained. The slope is a measurement of the contribution of diffusion process, so, diffusion process of inner surface contributes most of capacitance at a low scan rate. Obviously, $k_d > k_e$, at a high scan rate, the electrolyte can hardly enter into the gaps between the uniform nanoparticles and the micropores on the particles. As a result, it cannot make full use of inner surface area, which makes much contribution to the capacitance.
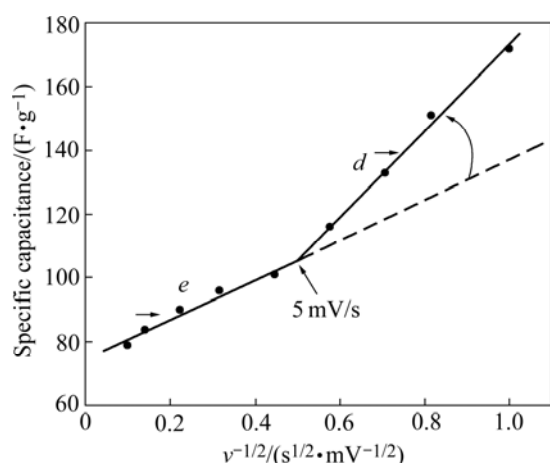


**Fig.5** Relationship between scan rate and specific capacitance of γ-Mo₂N in 1 mol/L H₂SO₄

We also obtain that $k_d/k_e$=2.5 from the plot, considering that the ratio of specific surface areas is reciprocal to that of radius, and the value of $k_d/k_e$ is near to $r_2/r_1$ ($r_2$ is the radius obtained from TEM results while $r_1$ is from XRD results). The consequence matches the results of XRD and TEM. The difference between them exists possibly due to the incomplete use of inner surface.

All the conclusions mentioned above also reveal that we can modulate the experimental conditions to control the particle size and distribution of micropore diameters of the electrode material in order to get high specific capacitance in further investigation.

3.3.3 Effect of electrolytes on specific capacitance

Fig.6 gives the cyclic voltammogram(CV) curves of γ-Mo₂N electrode at a scan rate of 10 mV/s in 1 mol/L H₂SO₄, 1 mol/L KCl, 1 mol/L H₂SO₄ and 3 mol/L H₂SO₄ aqueous solution, respectively. As seen in Fig.6, the γ-Mo₂N electrode exhibits rectangular shape curves in these aqueous electrolytes. The data indicate that the γ-Mo₂N electrode has a good capacitive behavior in the potential range of (−0.6−0.5) V (vs SCE) in H₂SO₄ aqueous electrolyte, and (−0.5−0.4) V (vs SCE) in KCl electrolyte.
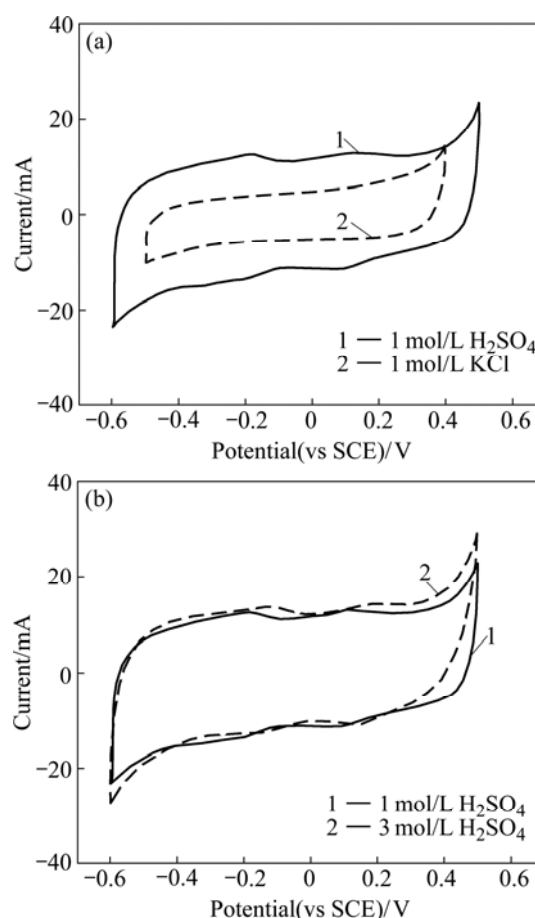
Electrochemical performances of γ-Mo₂N electrode



**Fig.6** CV curves of γ-Mo₂N electrode in different electrolytes (a) and in different concentration of H₂SO₄ electrolyte (b)

in different electrolytes are listed in Table 1. As can be clearly observed in Fig.6 and Table 1, the CV curves of γ-Mo₂N electrode display more symmetric rectangular shape and larger output current in H₂SO₄ solutions than in KCl solutions, revealing that γ-Mo₂N electrode has better capacitive performance in H₂SO₄ solutions. The reason may be that the conductivity of H₂SO₄ is better than that of KCl electrolyte, and the radius of water hydration of H⁺ is a little smaller than that of K⁺, so the material allows an easier access of H⁺ to the electrode/electrolyte interface. When the scan rate is relatively slow, the material in H₂SO₄ can more easily and fully contact with the electrolyte. Electrolyte resistance and contact resistance may be other factors. The results also demonstrate differences of potential window in different electrolytes. The minimum limit in 1 mol/L H₂SO₄ (−0.6 V) is lower than that in 1 mol/L KCl (−0.5 V), and the maximum limit in 1 mol/L H₂SO₄ (0.5 V) is also higher than that in 1 mol/L KCl (0.4 V). Obviously, concentration of the two electrolytes does not affect much on the electrochemical performance.

3.3.4 Cycle life

In Fig.7, the ratio of the initial specific capacitance of the electrode material is given as a function of cycle

**Table 1** Electrochemical performances of $\gamma$-Mo$_2$N electrode in different electrolytes

| Electrochemical performance | $c(KCl)/(mol\cdot L^{-1})$ | | $c(H_2SO_4)/(mol\cdot L^{-1})$ | |
|---|---|---|---|---|
| | 1 | 3 | 1 | 3 |
| Potential window/V | −0.5−0.4 | −0.5−0.4 | −0.6−0.5 | −0.6−0.5 |
| $C/(F\cdot g^{-1})$ | 103.2 | 100.8 | 172.0 | 171.0 |
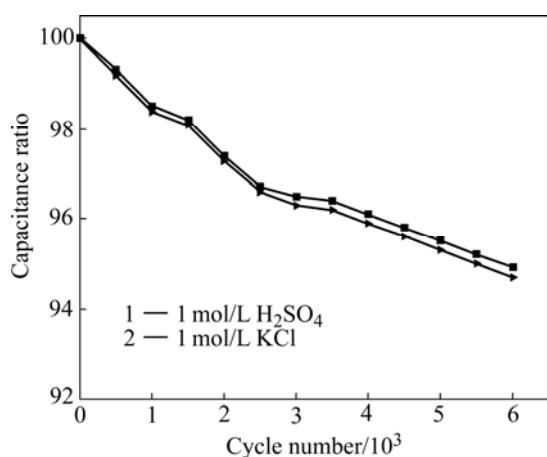


**Fig.7** Cycle-life of capacitors based on $\gamma$-Mo$_2$N (scan rate: 100 mV/s)

number. At the 6 000th cycle, the specific capacitance remains about 94.9% of the initial in the electrolyte of 1 mol/L H$_2$SO$_4$, while it remains 94.7% in 1 mol/L KCl solution. Obviously, the as-prepared $\gamma$-Mo$_2$N has better stability in 1 mol/L H$_2$SO$_4$, in addition, it is clear that the loss of specific capacitance of the electrode material is nearly 3.6% during the former 3 000 cycles, but only 1.4% during the last 3 000 cycles. In other words, the decreasing rate is much slower as the cycle numbers increase. In a word, this material has long durability in both two electrolytes.

3.3.5 AC impedance

The typical impedance spectrum of the electrode at different potentials are shown in Fig.8. Impedance spectra were recorded with 5 mV AC perturbation in the frequency range from 10 kHz to 10 mHz. Considering the better capacitive performance in H$_2$SO$_4$ electrolyte, the impedance investigation was taken in 1 mol/L H$_2$SO$_4$. On the whole, the Nyquist plots of $\gamma$-Mo$_2$N electrode at the two potentials are similar to each other. A suppressed semicircle may exist in the higher frequency range followed by the steep rising line at the lower frequency range, where their behaviors are mainly capacitive. In most cases, the depressed semicircles are usually considered small charge transfer resistances between electrode and electrolyte[20]. In high frequency intercept of the real axis, an internal resistance can be observed, which is composed of the resistance of the electrolyte, the intrinsic resistance of the electrode material and

contact resistance at the interface between the active material and current collector[21]. The resistances of the electrolyte are both calculated to be 2.55 Ω at the two different potentials in our experiment. The change of potential may have influence on the surface property of the active material, especially for the nanopore structure. Therefore, it will possibly lead to the change of resistance. The line in low frequency range has a finite slope, representing the diffusive resistivity of the electrolyte within the pore of the electrode[22]. The imaginary part of the impedance increases in the low frequency range in Fig.8, which indicates the capacitive behavior of supercapacitor[21]. The two plots at different potentials show few differences, illuminating that potential does not affect much on the impedance performance of the $\gamma$-Mo$_2$N electrode.
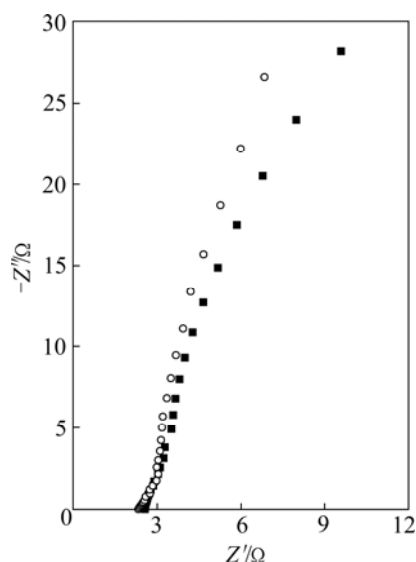


**Fig.8** Typical impedance spectra of $\gamma$-Mo$_2$N electrode in 1 mol/L H$_2$SO$_4$

# 4 Conclusions

1) Uniform nanoparticles of $\gamma$-Mo$_2$N with a narrow size distribution and average size of about 16 nm were prepared via the nitridation of MoO$_3$ by TPR method. The relationship between scan rate and specific capacitance can be explained by the mixed mechanism of surface control and diffusion control. The high specific capacitance is attributed to the ultrafine and uniform structure of $\gamma$-Mo$_2$N and uniform particle distribution plays an important role in improving performance of supercapacitor materials.

2) The as-prepared material has good electrochemical performance with a high specific capacitance of 172 F/g and a broadened potential window ranging from −0.6 V to 0.5 V in 1 mo/L H$_2$SO$_4$ electrolyte.

3) This as-prepared material possesses long durability and excellent stability with the ratio of capacitance remaining 94.9% and 94.7% in 1 mol/L $H_2SO_4$ and 1 mol/L KCl solution, respectively, the 6 000th cycle.

# References

[1]   KOTZ R, CARLEN M. Principles and applications of electrochemical capacitors [J]. Electrochim Acta, 2000, 45(15/16): 2483−2498.

[2]   GOUEREC P, TALBI H, MIOUSSE D, TRAN-VAN F, DAO L H, LEE K H. Preparation and modification of polyacrylonitrile microcellular foam films for use as electrodes in supercapacitors [J]. J Electrochem Soc, 2001, 148(1): A94−A101.

[3]   LI Xue-liang, LI Wen-jie, CHEN Xiang-ying, SHI Cheng-wu. Hydrothermal synthesis and characterization of orchid-like $MnO_2$ nanostructures [J]. J Cryst Growth, 2006, 297(2): 387−389.

[4]   LIU Kai-yu, ZHANG Ying, ZHANG Wei, ZHENG He, SU Geng. Charge-discharge process of $MnO_2$ supercapacitor [J]. Trans Nonferrous Met Soc China, 2007, 17(3): 649−653.

[5]   ZHENG Yan-zhen, ZHANG Mi-lin. Preparation and electrochemical properties of nickel oxide by molten-salt synthesis [J]. Mater Lett, 2007, 61(18): 3967−3969.

[6]   HUANG L M, LIN H Z, WEN T C, GOPALAN A. Highly dispersed hydrous ruthenium oxide in poly(3,4-ethylenedioxythiophene)-poly(styrene sulfonic acid) for supercapacitor electrode [J]. Electrochim Acta, 2006, 52(3): 1058−1063.

[7]   ZHENG J P, CYGAN P J, JOW T R. Hydrous ruthenium oxide as an electrode material for electrochemical capacitors [J]. J Electrochem Soc, 1995, 142(8): 2699−2703.

[8]   HU Chi-chang, HUANG Yao-huang. Cyclic voltammetric deposition of hydrous ruthenium oxide for electrochemical capacitors [J]. J Electrochem Soc, 1999, 14(7): 2465−2471.

[9]   HU C C, CHANG K H. Cyclic voltammetric deposition of hydrous ruthenium oxide for electrochemical capacitors: Effects of codepositing iridium oxide [J]. Electrochim Acta, 2000, 45(15/16): 2685−2696.

[10]  LUO Fang-chen, CHEN Qi-yuan, YIN Zhou-lan. Electrochemical performance of multiphase nickel hydroxide [J]. Trans Nonferrous Met Soc China, 2007, 17(3): 654−658.

[11]  CHEN Chang-lun, ZHAO Dong-lin, WANG Xiang-ke. Influence of addition of tantalum oxide on electrochemical capacitor performance of molybdenum nitride [J]. Mater Chem Phys, 2006, 97(1): 156−161.

[12]  CHEN Chang-lun, ZHAO Dong-lin, XU Di, WANG Xiang-ke. $\gamma$-$Mo_2N$/$Co_3Mo_3N$ composite material for electrochemical supercapacitor electrode [J]. Mater Chem Phys, 2006, 95(1): 84−88.

[13]  LI Xue-liang, CHEN Xue-ji, CHEN Xiang-ying, HAN Chang-long, SHI Cheng-wu. Hydrothermal synthesis and characterization of $VO_2$ (B) nanorods array [J]. J Cryst Growth, 2007, 309(1): 43−47.

[14]  NAGAI M, GOTO Y, MIYATA A, KIYOSHI M, HADA K, OSHIKAWA K. Temperature-programmed reduction and XRD studies of ammonia-treated molybdenum oxide and its activity for carbazole hydrodenitrogenation [J]. J Catal, 1999, 182(2): 292−301.

[15]  NAGAI M, YAMAMOTO Y, AONO R. Surface properties and fractal approach to molybdenum nitrides and their surface activity for hydrodenitrogenation [J]. Colloids Surf A: Physicochem Eng Aspects, 2004, 241(1/3): 257−263.

[16]  RANHOTRA G S, HADDIX G W, BELL A T, REIMER J A. Catalysis over molybdenum carbides and nitrides (I): Catalyst characterization [J]. J Catal, 1987, 108(1): 24−39.

[17]  KIM D W, LEE D K, IHM S K. CoMo bimetallic nitride catalysts for thiophene HDS [J]. Catal Lett, 1997, 43(1/2): 91−95.

[18]  LIU T C, PELL W G, CONWAY B E, ROBERSON S L. Behavior of molybdenum nitrides as materials for electrochemical capacitors [J]. J Electrochem Soc, 1998, 145(6): 1882−1888.

[19]  CULLITY B D. Element of X-ray diffraction [M]. Massachusetts: Addison-Wesley, 1978.

[20]  QU Q T, WANG B, YANG L C, SHI Y, TIAN S, WU Y P. Study on electrochemical performance of activated carbon in aqueous $Li_2SO_4$, $Na_2SO_4$ and $K_2SO_4$ electrolytes [J]. Electrochem Commun, 2008, 10(10): 1652−1655.

[21]  HE Xiao-jun, JIANG Li, YAN Shan-cheng, LEI Jiang-wei, ZHENG Ming-dong, SHUI Heng-fu. Direct synthesis of porous carbon nanotubes and its performance as conducting material of supercapacitor electrode [J]. Diamond & Relat Mater, 2008, 17(6): 993−998.

[22]  KIM C, CHOI Y O, LEE W J, YANG K S. Supercapacitor performances of activated carbon fiber webs prepared by electrospinning of PMDA-ODA poly(amic acid) solutions [J]. Electrochim Acta, 2004, 50(2/3): 883−887.

**(Edited by YANG Hua)**